



Higher mode effects of multistorey substructures on the seismic response of double-layered steel gridshell domes

Deepshikha Nair^{*}, Keita Ichihashi, Yuki Terazawa, Ben Sitler, Toru Takeuchi

Tokyo Institute of Technology, Tokyo, Japan

ARTICLE INFO

Keywords:

Gridshell roofs
Seismic response
Domes
Higher mode effects
Amplification factors
Equivalent static loads
Multistorey substructures

ABSTRACT

The seismic response of gridshell roofs with substructures is strongly influenced by the relative mass and stiffness of the roof and substructure, and particularly by how close the periods of the dominant roof and substructure modes are. Multistorey substructures may exhibit a significant higher-mode acceleration response, primarily due to the contribution of the shorter second translational substructure mode to the roof response. This paper presents parametric studies conducted on steel gridshell domes with 60, 100 and 150 m spans and six-storey substructures to investigate the interaction between the higher substructure modes and dominant roof modes. The contribution of each substructure mode to the overall response was characterised by a newly proposed dominance response ratio. In contrast to previous studies of long-period single-storey substructures, which only minimally excited the roof modes, the higher modes of the long-period multistorey substructures investigated in this study significantly contributed to the roof response. The roof vertical accelerations were amplified by up to three times the substructure roofline acceleration, as the curved roof geometry couples the horizontal substructure and vertical roof response. The substructure higher-mode contribution was quantified using amplification factors and developed into equivalent static loads that were found to be in good agreement with response spectrum analysis results. The proposed equivalent static loads provide insight into the complex dynamic characteristics of gridshell roofs with multistorey substructures and offer an efficient method for preliminary seismic design.

1. Introduction

Gridshell roofs offer a unique structural topology capable of achieving long spans with minimal structural materials. The analysis and design of short-span single-layer gridshell roofs is often governed by static gravity loads and buckling limit states, which have been widely studied in literature [1–4]. However, the dynamic response under earthquake actions results from a complex interaction of multiple roof and substructure modes and is less well established, but nevertheless critical to the design of gridshells in areas of high seismic hazard. Previous studies of raised single-layer cylindrical gridshells [5,6] have indicated that the dynamic characteristics are influenced by the rise-to-span ratio, length-to-span ratio and the fundamental anti-symmetric mode.

Extensive non-structural damage to the ceilings and suspended services during recent major earthquakes in Japan [7,8] has included buckled or fractured lattice members, collapsed ceilings and fractured

boundary connections, and has rendered school gymnasiums, sports facilities and convention centres incapable of fulfilling their intended use as emergency post-earthquake shelters [9]. This has been primarily attributed to large out-of-plane roof accelerations resulting from horizontal earthquake ground motion, which is amplified up the substructure and excites the vertical asymmetric modes of curved roofs. Extensive non-structural and local structural damage impairs the ability of gymnasiums, sports facilities and convention centres to function as post-earthquake emergency shelters [8]. In response to this performance, researchers have investigated the collapse mechanisms and seismic fragility of gridshell domes [10,11]. Nie et al. [12] performed incremental dynamic analyses to obtain the seismic fragility curves for single-layer reticulated domes and found that failure was primarily related to the dynamic strength. Furthermore, the response sensitivity of domes has been investigated by Pokusiński et al. [13] and by Zhong et al. [14], who concluded that the seismic response was most sensitive to the structural damping, yield strength and the ultimate strain.

^{*} Corresponding author.

E-mail addresses: nair.d.aa@m.titech.ac.jp (D. Nair), ichihashi.k.ab@m.titech.ac.jp (K. Ichihashi), terazawa.y.aa@m.titech.ac.jp (Y. Terazawa), sitler.b.aa@m.titech.ac.jp (B. Sitler), takeuchi.t.ab@m.titech.ac.jp (T. Takeuchi).

<https://doi.org/10.1016/j.engstruct.2021.112677>

Received 27 January 2021; Received in revised form 26 May 2021; Accepted 3 June 2021

0141-0296/© 2021 The Authors. Published by Elsevier Ltd. This is an open access article under the CC BY license (<http://creativecommons.org/licenses/by/4.0/>).

A consequence of the unique dynamic characteristics is that the seismic analysis and design of gridshell roofs differ from multistorey buildings [15,16], which are the primary focus of most design codes. For example, ASCE-7-16 [17], NZS1170.5 [18], Eurocode 8 [19] and the Building Standard Law of Japan [20] all prescribe an equivalent lateral force method for simple multistorey structures, and use this as a baseline for more complex analysis methods. Despite differences between codes, each estimate horizontal inertial storey forces from the storey masses, fundamental period, assumed vertical distribution and inelastic design spectra, which is calculated using a response reduction (R [17], F_h [20]) or ductility factor (k_μ [18]). Tall or irregular structures may be designed using modal response spectrum analysis (RSA) [17–19], but the design forces are still limited by the equivalent lateral force method, and higher modes are generally assigned the same response reduction factor for simplicity. The equivalent lateral force distribution also provides the basis for some nonlinear pushover methods [17,20]. However, these codes provide minimal commentary on what response reduction factor to use for gridshells, where higher modes may generate significant excitation, nor is it apparent how equivalent lateral forces developed for multistorey buildings should be applied [16,21]. Consequently, RSA is often used as the baseline analysis method, as it is the simplest method that captures the coupled horizontal substructure-vertical roof response. However, RSA requires a high degree of expertise due to the complex, closely spaced modes and sensitivity of the substructure-roof interaction to the precise modelling assumptions.

Nevertheless, previous researchers have proposed equivalent static forces for single- and double-layered lattice domes with single-storey substructures based on the interaction between the fundamental substructure sway mode and dominant roof anti-symmetric mode [22,23]. Equivalent lateral forces have also been proposed for medium-span domes with single-storey substructures using amplification factors, considering four predominant roof modes [24]. This method estimates the horizontal and vertical equivalent roof forces from the horizontal acceleration at the substructure roof level, roof nodal masses, modeshape-specific acceleration distributions and amplification factors that increase with the proximity of the substructure and roof modes. Later studies found this method to be accurate for a medium-span dome roof with a triple storey substructure where the substructure mass participation was dominated by the fundamental mode [25]. A similar approach was proposed by Khalili et al. [26], who studied single-layer barrel vaults (20–30 m span) and proposed behaviour and displacement amplification factors as functions of the rise-to-span ratio. Jamshidi et al. [27] conducted pushover analysis using a special horizontal load pattern to account for higher modes, and obtained capacity curves for double-layer lattice domes. The amplification factor approach was recently adopted in a design manual published by IASS [21] for the preliminary seismic design of medium-span domes and cylindrical gridshells with single-storey substructures. Note that these studies were limited to elastic structures, although equivalent static forces have also been proposed for single-storey substructures with energy dissipation devices [23,28].

While these equivalent static force proposals cover typical cases such as school gymnasiums and small indoor arenas, they neglect higher substructure modes, which may be close to the dominant roof modes and exhibit significant mass participation for multistorey substructures. The authors previously investigated the interaction of 150 m long-span domes with multistorey substructures, which alternatively incorporated spine frames and buckling-restrained braces [29]. Despite reducing the roof response associated with the fundamental substructure mode, the elastic higher substructure modes interacted with the roof and significantly amplified the response. While confirming the substantial influence of higher substructure modes on the roof response for multistorey substructures, the same amplification factor curves were used for the roof interaction with both the first and second substructure modes. However, a wide range of ratios between the higher substructure and roof modes are conceivable, and the previously developed

amplification factor curves [24] may need to be refined to avoid a gross overestimation or underestimation of the roof response.

The present study investigates the effects of higher substructure modes on the roof response and develops amplification factors for dome gridshell roofs with multistorey substructures. A parametric study was performed for 60, 100 and 150 m double-layered domes featuring a range of substructure stiffness and roof-substructure mass ratios using response spectrum analysis. The overall response contribution of the dominant substructure mode, which need not be the fundamental substructure mode, was investigated using a new ‘dominance response ratio’ that provides insight into the dynamic roof-substructure interaction. Horizontal and vertical amplification factors were proposed to estimate the roof response generated by higher multistorey substructure modes. The proposed amplification factors were then applied to obtain combined roof accelerations, which may be used to design acceleration-sensitive non-structural components. A generalised equivalent static design procedure was then developed for domes with multistorey substructures and validated against RSA, comparing against both the nodal displacements and member forces.

2. Analysis models

Prototype medium- and long-span double-layered dome roofs were selected, as double-layered lattices exhibit less complex dynamic characteristics than the single-layer lattices and are ubiquitous in high seismic regions. Double-layered domes with depth-to-span (d/L where d is the vertical offset and L is the span) ratios exceeding $1/50$ [24] exhibit four primary modes, with the three primary out-of-plane modes denoted ‘O1’, ‘O2’ and ‘O2.5’, and the in-plane mode ‘I’ (Fig. 1). Three roof models (Table 1) with 60, 100 and 150 m spans and a half subtended angle (θ) of 30° were designed using SN490 steel ($f_y = 325$ MPa) for three different dead loads (2, 2.44 and 3 kPa), respectively (Fig. 2 (a)). The roof dead loads were determined considering a structural weight of about 1 kg/m^2 for every meter of span [30], a 15% allowance for the connections, and 1.3 kPa nonstructural dead load, such as purlins, cladding, ceilings, mechanical and electrical. The double-layer lattice member sizes and vertical offsets (d) between the section centerlines are listed in Table 1. For simplicity, the double-layer lattice (Fig. 1(a-iii)) was modelled using equivalent beams with out-of-plane stiffness modification factors and moment connections (Fig. 1(a-iv)). The equivalent beam sizes were determined as shown in Fig. 1(a) such that the area of the beam (A) equals the combined area of the two sections of the double-layer lattice ($2 \times A/2$). The moment of inertia of the equivalent beam in the out-of-plane direction I_{3s} was then increased by a modification factor m to match the moment of inertia of the double-layer lattice about the centerline I_{3d} . All roof members were modelled as elastic beam elements, which is consistent with the common design philosophy where the roof lattice is designed to remain elastic [21]. Partial models omitting the substructure and pinning the roof lattice perimeter nodes were used to identify the roof modes and are denoted as ‘roof models’. The roof geometry was modelled in *Grasshopper* [31] and imported to ETABS [32] for analysis. The roof member beams in ETABS were modelled as ‘frame’ objects which are general three-dimensional beam elements [33] including axial, biaxial shear, torsion and biaxial bending deformation [34].

The lateral force resisting system of the substructure consisted of a two-way moment-resisting frame (MRF) enveloping 24 circumferential bays of buckling-restrained braced frames (BRBFs) spaced equidistantly along the perimeter, as shown in Fig. 2(b). The substructure was designed to keep the MRF elastic, with the maximum inter-storey drift limited to 1% under a Japanese level-2 [20] earthquake (comparable to the design basis earthquake, DBE) on the West Coast, US [35]. Therefore, the beams and columns were modelled using elastic beam elements with the section sizes listed in Table 2(b). The BRBs (arranged in a single-diagonal configuration for the shorter beam spans of the 60 m and 100 m models and chevron configuration for the longer beam spans of

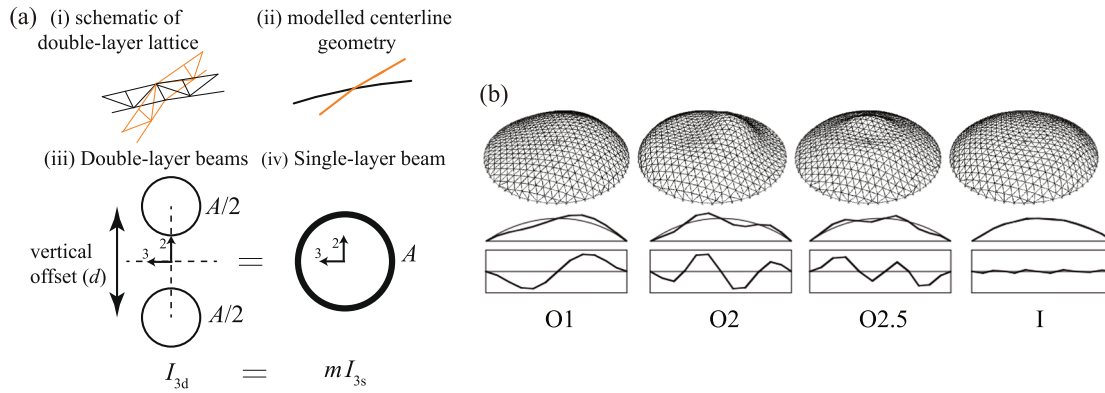


Fig. 1. (a) Equivalent single-layer beam modelling & (b) Four primary modes of a double-layered dome.

Table 1

Roof models: Member section sizes.

Model	Dead Load (DL) (kPa)	Double-layer beam (mm)	offset d (cm)	Single-layer beam (roof member) (mm)	m	Tension beam (mm)
L60	2	$2 \times 1250 \times 125 \times 6 \times 9^{**}$	150	$\phi 307.5 \ t 7.5^*$	53.3	$\phi 809 \ t 9$
L100	2.44	$2 \times 1250 \times 250 \times 9 \times 14$	200	$\phi 414.5 \ t 14.5$	50.7	$\phi 1020 \ t 10$
L150	3	$2 \times \phi 511 \ t 11$	350	$\phi 715.5 \ t 15.5$	51	$\phi 2525 \ t 25$

**I = I beam section, Dimensions: Height \times Breadth \times Web thickness \times Flange thickness

* ϕ = Outer Diameter, t = Thickness of circular hollow section

the 150 m models) were proportioned using Kasai's damper distribution method [36], which targets a uniform inelastic storey drift up the building height. However, this study is focused on the general dynamic substructure-roof interaction and so the complexities of a yielding substructure were omitted. Therefore, BRBs were modelled as elastic link elements using the initial axial stiffness (Table 2(a)). Note that although yielding may reduce the substructure response and elongate the first mode, this is an acceptable simplification as each roof-substructure mode pair is analysed separately. The focus of this study is to quantify the roof amplification where multiple substructure modes contribute to the response, and inelasticity is outside the scope of the present study. Nevertheless, it is anticipated that the proposed amplification factors will remain valid for a yielding multistorey substructure as well.

Finally, the substructure floors were modelled as membrane elements and assigned as rigid diaphragms [32]. A 7 kPa uniform load was applied to all floors, giving the storey seismic weights listed in Table 2(a). To isolate the effect of the horizontal substructure acceleration on the roof response, a tension ring beam was included along the roof perimeter and pinned connections provided to both the substructure framing members and roof lattice, eliminating the local bending moments that would otherwise occur (Fig. 2(c)). Furthermore, the cantilever columns at the top storey were braced in the radial direction to avoid a soft storey.

As a complement to the 'roof model', a 'substructure model' was analysed where the roof gridshell was replaced with a rigid diaphragm and lumped mass (Fig. 2(b)). A third 'combined model' was then constructed that includes both the roof gridshell and substructure (Fig. 2(c)). The two partial models were solely used to obtain the independent modal properties of the roof and substructure, while the combined model was used to obtain the seismic response and validate the analytical procedure.

3. Single-storey substructures

Before investigating the response of the multistorey models, the first-mode response characteristics were confirmed using single-storey

substructure models to benchmark the response. The fundamental response characteristics are further clarified by first reviewing the amplification factor, demonstrating how the analytical response of a simple arch model relates to more complex 3-d behaviour of the models investigated in this paper.

3.1. Amplification factor approach

Seismic response amplification factors were previously derived analytically for a simple 2-d arch model by Takeuchi et al. [24]. The arch model shown in Fig. 3 has three masses, spring hinges and rigid axial stiffness, which captures the asymmetric out-of-plane mode shape that generally governs the dynamic response. The modal participation factor (β_{R1}) and effective mass (M_{R1}) of the asymmetric out-of-plane mode are expressed in Eqs. (1) and (2), where m is the diagonal nodal mass matrix and I_x is the identity vector with the x components. The in-plane effective mass (M_{R2}) is then given by Eq. 3. This captures the modal mass of the axial vibration modes, but since the axial stiffness is assumed to be infinite [24], the spectral acceleration of these modes is identical to the input ground acceleration ($S_{A2} = S_{Ag}$).

$$u^T = u \left[\sin \frac{3}{4}\theta, -\cos \frac{3}{4}\theta, 2\sin \frac{\theta}{4}, 0, \sin \frac{3}{4}\theta, \cos \frac{3}{4}\theta \right] \quad (1a)$$

$$u = 2R a \sin \frac{\theta}{4} \quad (1b)$$

$$\beta_{R1} = \frac{u^T m I_x}{u^T m u} = \frac{\sin \frac{3}{4}\theta + \sin \frac{\theta}{4}}{u \left(1 + 2\sin^2 \frac{\theta}{4} \right)} \quad (2a)$$

$$M_{R1} = \frac{(u^T m I_x)^2}{u^T m u} = \frac{2m \left(\sin \frac{3}{4}\theta + \sin \frac{\theta}{4} \right)^2}{1 + 2\sin^2 \frac{\theta}{4}} \quad (2b)$$

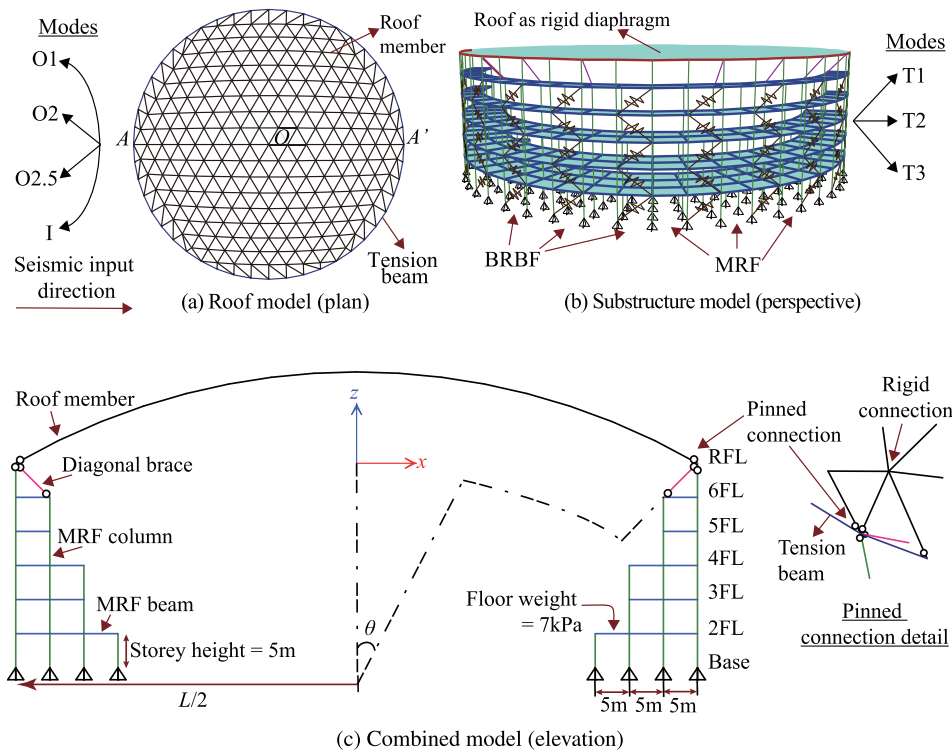


Fig. 2. Multistorey models.

Table 2

Substructure model data.

(a) Storey weight distribution and BRB stiffness							
Storey	Height (m)	Seismic weight (kN)			BRB axial stiffness (kN/m)		
		L=60	L=100	L=150	L=60	L=100	L=150
RFL	30	6063	20581	56840	108989	-	-
6FL	25	6032	10420	15904	80057	101373	271382
5FL	20	6032	10420	15904	118111	225316	314543
4FL	15	10968	19742	30710	149529	318357	252994
3FL	10	10968	19742	30710	287434	442784	367798
2FL	5	10968	27968	44420	472209	598652	626060
Total		51031	108873	194488			

(b) MRF section sizes				
Member	Section shape	Section sizes (mm)		
		L=60	L=100	L=150
MRF column	SHS*	450×450×25	600×600×32	650×650×32
MRF beam	I/Wide flange**	340×250×9×14	450×300×10×16	550×400×20×25
Diagonal brace	SHS*	350×350×15	350×350×16	200×200×8

*SHS=square hollow section, Dimensions: Height×Breadth×Thickness

**I=I section, Dimensions: Height×Breadth×Web thickness×Flange thickness

$$M_{R2} = M_R - M_{R1} = 3m \left(1 - \frac{2 \left(\sin \frac{3}{4} \theta + \sin \frac{\theta}{4} \right)^2}{3 \left(1 + 2 \sin^2 \frac{\theta}{4} \right)} \right) \quad (3)$$

The out-of-plane modal mass M_{R1} increases with the half-subtended angle θ , which corresponds to a greater contribution from the asymmetric out-of-plane mode, while M_{R1} reduces to zero when $\theta = 0$. The maximum response of the roof can thus be expressed by combining the base ground motion and out-of-plane mode's response. The response amplification factors are defined as the response of roof divided by the base acceleration, which is equal to the peak ground acceleration S_{Ag} . Assuming the asymmetric mode T_R lies on the constant acceleration region of the spectrum such that $S_{A1} = S_{AP}$ [24], the amplification

factors F_H and F_V may be derived as the horizontal and vertical components of F in Eq. (4). These equations have been previously validated using CQC and linear response history analyses [24].

$$A_R = \sqrt{\left(S_{A1} \beta_{R1} u \right)^2 + \left(S_{A2} I_x \left(\frac{M_{R2}}{M_R} \right) \right)^2} \quad (4a)$$

$$F = \frac{A_R}{S_{Ag}} = \sqrt{\left(\frac{S_{AP}}{S_{Ag}} \beta_{R1} u \right)^2 + \left(I_x \left(\frac{M_{R2}}{M_R} \right) \right)^2} \quad (4b)$$

This method was extended for raised roofs using the substructure-roof representation depicted in Fig. 4 [24]. The amplification factors for these cases are given by Eq. 5, which replaces the ground acceleration with the maximum acceleration at the top of the substructure A_{eq} and

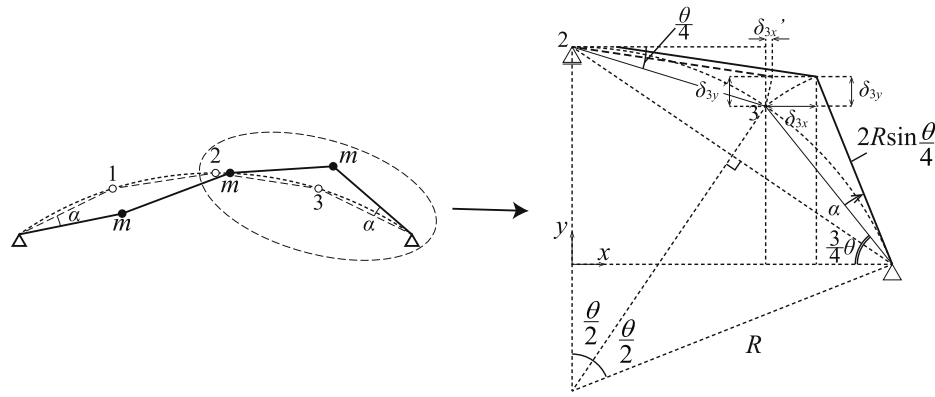


Fig. 3. Asymmetric mode of the 2-d arch model [24].

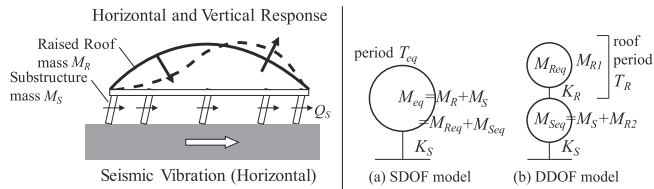


Fig. 4. Raised roof response and combined model as an equivalent DDOF model [24].

S_{A1} with the spectral acceleration of the out-of-plane modal roof mass M_{R1} ($S_{A1} = S_{AR1}$) [24]. The equations were validated against response spectrum analyses results and linear response history analyses [24].

$$F = \frac{A_R}{A_{eq}} = \sqrt{\left(\frac{S_{AR1}}{A_{eq}} \beta_{R1} u\right)^2 + \left(I_x \left(\frac{M_{R2}}{M_R}\right)\right)^2} \quad (5)$$

The same concept was then extended to more complex 3-d domes and cylindrical roofs with single-storey substructures using 3-d models modelled using beam elements. Since multiple roof modes (O1, O2, O2.5 and I) contribute to the overall response, the amplification factors were obtained using results directly obtained from the response spectrum analyses. Simple horizontal and vertical amplification factor curves were proposed by dividing the peak roof response by the peak sub-

structure response [24]. Section 5 applies the same fundamental concepts to domes with multi-storey substructures to study the roof-substructure interaction and quantify the effect of higher modes of the substructure on the roof response.

3.2. Mass and period ratios

The amplification factors arising from the roof-substructure interaction primarily depend on the mass (M_M) and period (R_T) ratios [24] defined in Eq. 6. These are formulated as ratios of the effective modal mass (${}_s M_{eqi}$) and period (${}_s T_i$) of the i^{th} mode of the substructure model, which includes the roof mass, relative to the total roof mass (${}_r M_R$) and period of the dominant O1 roof mode (${}_r T_R$). Therefore, a larger R_M or R_T ratio represents a heavier and more flexible substructure, such that both ratios increase as storeys are added. For completeness, the effective modal mass, mass participation factor (Γ_i) and modal participation factor (β_i) are given by Eq. (7), where m is the mass matrix and ϕ_i is the mode shape vector.

Note that the preceding subscripts r, s and c are used in this paper to refer to the roof, substructure and combined models (Fig. 2 and 5), respectively.

$$R_{Mi} = \frac{{}_s M_{eqi}}{{}_r M_R}, \quad R_M = \sum_{i=1}^n R_{Mi}, \quad R_{Ti} = \frac{{}_s T_i}{{}_r T_R} \quad (6)$$

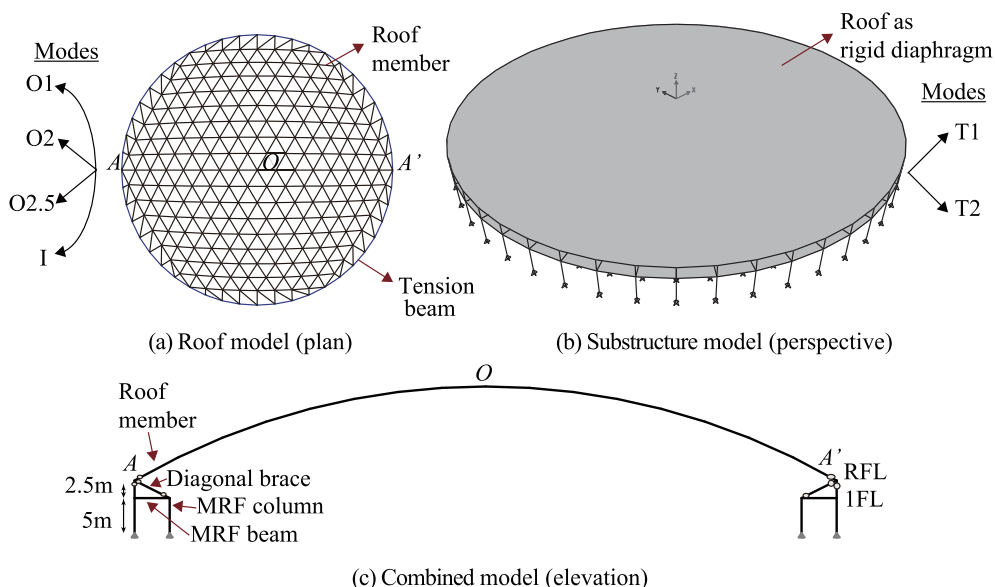


Fig. 5. Single-storey models.

$$\beta_i = \frac{\phi_i^T m \{1\}}{\phi_i^T m \phi_i} \quad (7a)$$

$${}_s M_{eqi} = \frac{(\phi_i^T m \{1\})^2}{\phi_i^T m \phi_i} \quad (7b)$$

$$\Gamma_i = \frac{{}_s M_{eqi}}{\sum_{i=1}^n {}_s M_{eqi}} \quad (7c)$$

3.3. Roof-substructure interaction

The effect of the mass (R_M) and period (R_T) ratios on the dynamic response are investigated in this section using the 100 m span models with single-storey substructures and a braced mezzanine (Fig. 5). The storey heights, seismic weight and frame sections are listed in Table 3 and Table 4. The total seismic weights were calculated using the surface areas and dead loads (DL) applied to the roof which varied from 1 to 3 kPa producing the roof periods listed in Table 4. Several different substructure stiffnesses were investigated by modifying the moment of inertia of the MRF beams and columns by a scale factor α , such that a higher α equates to a stiffer substructure. The periods and the mass participation factors of the first two substructure modes are given in Table 5. Here, the period ratio R_{T1} is the ratio of the first (T1) substructure mode's period (ranked in decreasing order of mass participation) to the roof's O1 period. Note that T2 includes all of the translational modes with a single inflection point, while T1 refers to the translational sway modes. However, T1 or T2 modes about all axes have identical periods for the dome models considered in this study due to symmetry.

Increasing the substructure stiffness decreased the fundamental periods of the combined model, but did not affect the cumulative mass participation factor of the modes featuring translational substructure sway, which was about 99% for most models (Table 5). This suggests that for first-mode dominated substructures, the roof response may be obtained from the peak acceleration at the substructure roofline (${}_s A_{Heq}$) generated solely from the first substructure mode, and that higher substructure modes need not be considered.

Eq. 8 defines the target design acceleration ($S_a(\text{cm}/s^2)$) spectrum where D_h is the reduction factor to adjust the damping ratio from the base damping ratio $h_b = 5\%$. The spectrum was adjusted to an inherent damping ratio $h_o = 2\%$ using Eq. 9 [20]. Mapping the periods of the roof and substructure models on the spectrum provides insight into their interaction (Table 6). The fundamental substructure mode always interacts with the nearest roof mode. For example, the fundamental substructure mode is much longer than all roof modes for the combined model with $R_M = 2.2$ (1 kPa) and $\alpha = 1/6$ (Table 6), and so the substructure T1 sway mode dominates while only mildly interacting with the roof's O1 mode (Table 7). Increasing the stiffness to $\alpha = 1$ brings the substructure and roof periods closer together and produces a strong interaction between the substructure T1 and roof O1 modes. This interaction manifests as two modes in the combined model, with the T1 and O1 modes interacting in and out of phase (denoted as O1 + T1 and O1-T1 in Table 7). Increasing the substructure stiffness by $\alpha = 6$ once

Table 3

L100: Single-storey substructure model data.

(a) Storey heights and seismic weights			(b) MRF section sizes		
Storey	Height (m)	Weight (kN)	Member	Section Shape	Section Size (mm)
RFL (3kPa)	2.5	25,230	MRF column	SHS	600×600×32
RFL (2kPa)		16,820	MRF beam	I/Wide flange	450×300×10×16
RFL (1kPa)		8,410	Diagonal brace	SHS	350×350×16
1FL	5	10,420			

Table 4

L100 roof models: Seismic weights, periods (s) and mass participation (%).

Roof dead load (kPa)	Weight (kN)	O1 (r, T_R)	O2	O2.5	I
1	8410	0.25s, (18%)	0.14s, (5%)	0.07s, (57%)	0.05s, (6%)
2	16820	0.35s, (18%)	0.20s, (5%)	0.11s, (57%)	0.07s, (6%)
3	25230	0.43s, (18%)	0.24s, (5%)	0.13s, (57%)	0.09s, (6%)

again produced dominant O1 + T1 and O1-T1 modes, although the cumulative participation factor of the O1 + T1 and O1-T1 modes reduced slightly to 93%, with another 5% participation coming from the next closest roof mode (O2) to the substructure sway mode (T1). Thus, the roof-substructure interaction is strongly influenced by the relative proximity of their fundamental periods, and the response of roofs with single-storey substructures may be explained solely from the interaction of a sequential subset of roof modes with the substructure T1 mode.

$$S_a(T) = \left\{ \begin{array}{ll} 350D_h(T/0.05)^{(1+\log(5/7)/\log 4)} & (T \leq 0.05) \\ 1000D_h & (0.05 < T \leq 0.2) \\ 1000D_h/(T/2\pi) & (0.2 < T < \pi/5) \\ & (\pi/5 \leq T) \end{array} \right\} \quad (8)$$

$$D_h = \sqrt{(1 + 75h_b)/(1 + 75h_o)} \quad (9)$$

4. Multistorey substructures

4.1. Parametric study: Varying substructure stiffness and mass ratios

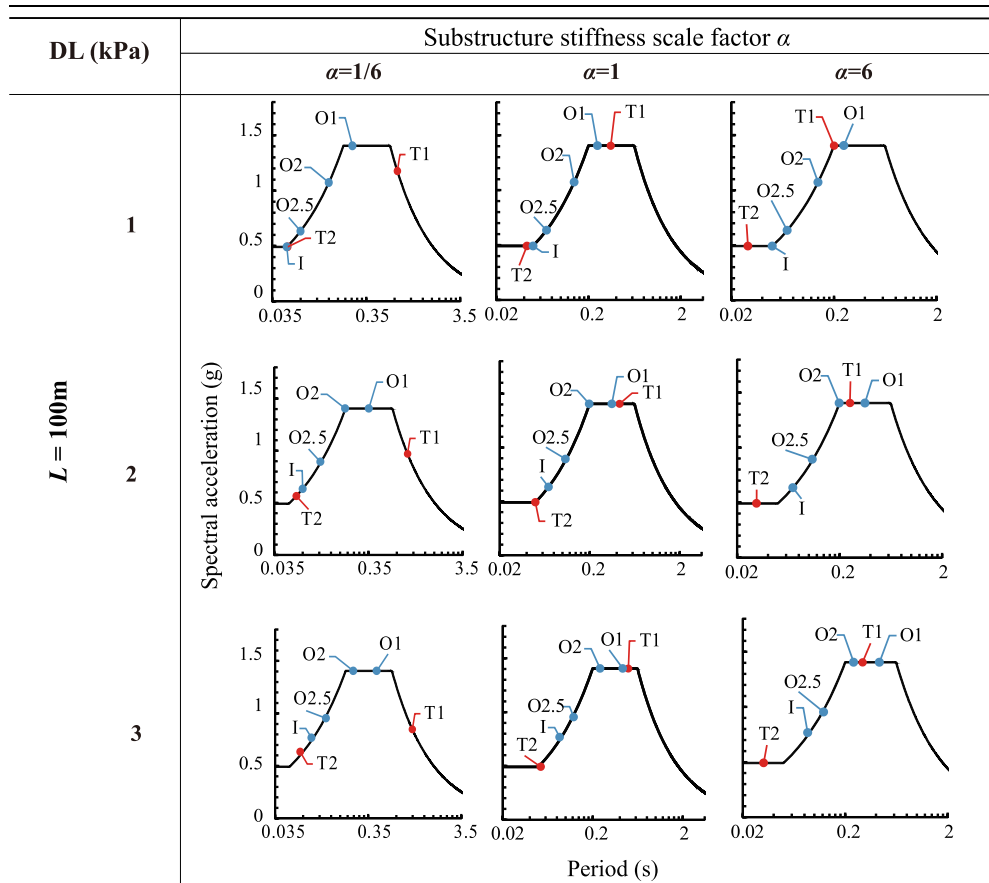
The multistorey substructure models defined in Section 2 are investigated in this section. As discussed in Section 3.2, the roof dead load ranged from 1 to 3 kPa, while the substructure loads were held constant and the substructure stiffness adjusted by modifying the moment of inertia of MRF members and axial stiffness of the BRBs by a scale factor α . Each model was labelled L-DL- κ where κ denotes the roof dead load (kPa).

The period ratios (R_{Ti}) and combined model mass participation factors (Γ_i) for the first two translational substructure mode shapes are plotted in Fig. 6. Here, the period ratios R_{T1} and R_{T2} are the ratios of the first (T1) and second (T2) substructure periods (ranked in decreasing order of mass participation) to the roof's O1 mode (r, T_R in Eq. 6 and Table 4). Note that the substructure modes are denoted by the mode shape, where T1 is a sway mode, while T2 and T3 feature increasing numbers of inflection points. Increasing the substructure stiffness decreased the period and participation factor of the first mode, indicating an increased contribution from the higher roof and substructure modes. The T1 modes have a mass participation factor of around $\Gamma_1 = 60\text{--}80\%$, with the remaining participation coming from the higher substructure modes. This implies that the peak acceleration of the substructure (${}_s A_{Heq}$) cannot be obtained solely from the substructure T1 mode, and that it may be important to include the contributions of the higher substructure modes, specifically those needed to achieve a minimum cumulative participation factor of 90% [17,19].

Table 5
Single-storey L100 substructure models: Periods (s) and mass participation (%).

Roof dead load (kPa)	R_M	α	T_1 and Γ_1 (%)	T_2 and Γ_2 (%)	R_{T1}
1	2.24	1/6	0.7s, (99%)	0.05s, (0.003%)	3.00
		1	0.3s, (99%)	0.04s, (0.5%)	1.40
		6	0.2s, (98%)	0.03s, (1.5%)	0.80
2	1.62	1/6	0.9s, (99%)	0.06s, (0.003%)	2.58
		1	0.4s, (99%)	0.05s, (0.5%)	1.22
		6	0.2s, (98%)	0.03s, (1.1%)	0.71
3	1.41	1/6	1.0s, (99%)	0.06s, (0.003%)	2.41
		1	0.5s, (99%)	0.05s, (0.4%)	1.15
		6	0.3s, (98%)	0.03s, (0.7%)	0.68

Table 6
Single-storey L100 models: Roof and substructure periods.

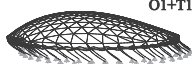

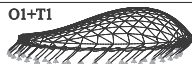
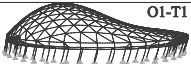
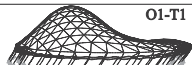
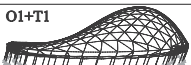
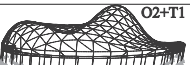
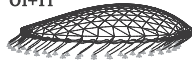
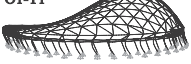
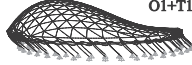

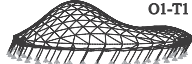
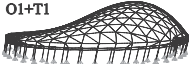

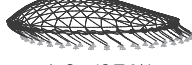
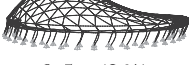
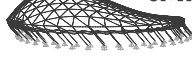

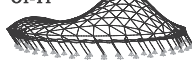
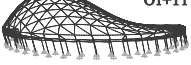



The roof and substructure periods are mapped on the design spectrum in Tables 8,9. Unlike the single-storey cases, both the substructure T1 and T2 modes interact with the nearest roof mode. For example, consider the mode shapes of the 100 m combined models shown in Table 10. For the combined model L100-DL-3 $\alpha = 1/6$, the first substructure mode (T1) is much longer than the roof modes (Table 9) and only weakly interacts with the roof O1 mode, as shown in Table 10. However, the substructure T2 mode strongly interacts with the roof O1 mode. Increasing the substructure stiffness to $\alpha = 1$ results in increased interaction between the substructure T1 and roof O1 modes, as well as between the substructure T2 and roof O2 modes, which have nearly identical periods. The third mode features the roof O1 mode mildly interacting with the substructure T1 mode. This trend is further

accentuated for the stiffer $\alpha = 6$ model, with the first and second modes exhibiting a strong interaction between the substructure T1 and roof O1 modes, but with a lower mass participation than the $\alpha = 1/6$ and 1 cases. The third mode features the substructure T2 mildly interacting with the roof's higher O2.5 mode.

Therefore, the dynamic characteristics of roofs with flexible multi-storey substructures ($\alpha = 1/6$ and $\alpha = 1/36$) are governed by the dominant roof mode O1 interacting with the closest substructure mode and the higher roof modes remain unexcited. On the other hand, when the T1 and T2 modes of stiffer multistorey substructures ($\alpha = 1$ and $\alpha = 6$) are closer to the O1 roof mode, the roof-substructure interaction is far more complex, exciting the O1, O2, O2.5 and I roof modes. Although the interacting pairs depend on the proximity of the respective substructure

Table 7
Single-storey combined models: Periods (s), mass participation (%) and mode shapes.

DL (kPa)	R_M	α	$L=100\text{m}$, Mode shapes		
1	2.2	1/6	 0.8s, (97%)	 0.3s, (1%)	-
		1	 0.4s, (89%)	 0.2s, (10%)	-
		6	 0.2s, (54%)	 0.3s, (39%)	 0.1s, (5%)
2	1.6	1/6	 1.0s, (97%)	 0.4s, (2%)	-
		1	 0.5s, (83%)	 0.3s, (15%)	-
		6	 0.2s, (55%)	 0.4s, (35%)	 0.2s, (4%)
3	1.4	1/6	 1.2, (97%)	 0.5s, (2%)	-
		1	 0.6s, (80%)	 0.4s, (18%)	-
		6	 0.3s, (54%)	 0.5s, (35%)	 0.2s, (5%)

and roof modes, combinations of the fundamental roof (O1 and O2) and substructure (T1 and T2) modes (e.g. O1 + T1, O2 + T2 and O1 + T2) tend to dominate. Furthermore, each substructure mode tends to be split into multiple combined modes, for example O1 + T1, O1-T1 and I + T1, each attracting a portion of the mass participation of the underlying substructure mode.

The seismic response of domes with multistorey substructures may therefore be interpreted as a combination of response from both T1-roof and T2-roof interactions. These interactions are further quantified in the following subsection.

4.2. Dominance Response Ratio

To distinguish the contributions of the substructure T1 and T2 modes to the peak response, a *dominance response ratio* DR_i is introduced. This ratio identifies the acceleration response contribution of the i^{th} substructure mode (cA_i) to the overall peak roof acceleration (cA_{SRSS}) calculated using the SRSS modal combination rule (Eq. 10). As the response is sensitive to the selected location, the horizontal and vertical ratios are reported at the node producing the maximum combined resultant response (usually a node near the quarter points). Therefore, DR_1 and DR_2 represent the combined response contribution of all modes exhibiting a substructure T1 or T2 mode, respectively.

$$DR_i = \frac{cA_i^2}{\left(\sqrt{\sum_{i=1}^n cA_i^2}\right)^2} = \frac{cA_i^2}{cA_{SRSS}^2} \quad (10)$$

Response spectrum analysis (RSA) was conducted for each combined model using the elastic BRI-L2 design spectrum [20] adjusted to a constant damping ratio of 2%. The dominance ratios in the horizontal and vertical directions were calculated using the critical node's acceleration results following Eq. 10 (Fig. 7). The horizontal dominance ratios were evenly divided between the T1 and T2 modes for longer period substructures, while the T1-roof interaction dominated for stiff substructures with $R_{T1} < 2$, with a horizontal T1 dominance ratio of $DR_1 > 80\%$. Furthermore, the vertical T1 dominance ratio DR_1 peaked at almost 100% for stiff substructures with $R_{T1} < 1$ such that the T1-roof interactions governed, but reduced for cases with $1 < R_{T1} < 2$ due to the increasing contribution of the T2-roof interactions and finally became negligible for flexible substructures with $R_{T1} \gg 2$, as the substructure period was too long for significant interaction. Similarly, the vertical T2 dominance ratio DR_2 peaked at almost 100% for $R_{T2} \approx 1$ and became negligible for longer substructure periods with $R_{T2} \gg 2$. This suggests that the vertical response contributions are more sensitive to the period ratios for multistorey structures and the vertical roof response is primarily a result of the T1-roof and T2-roof interactions for all but the

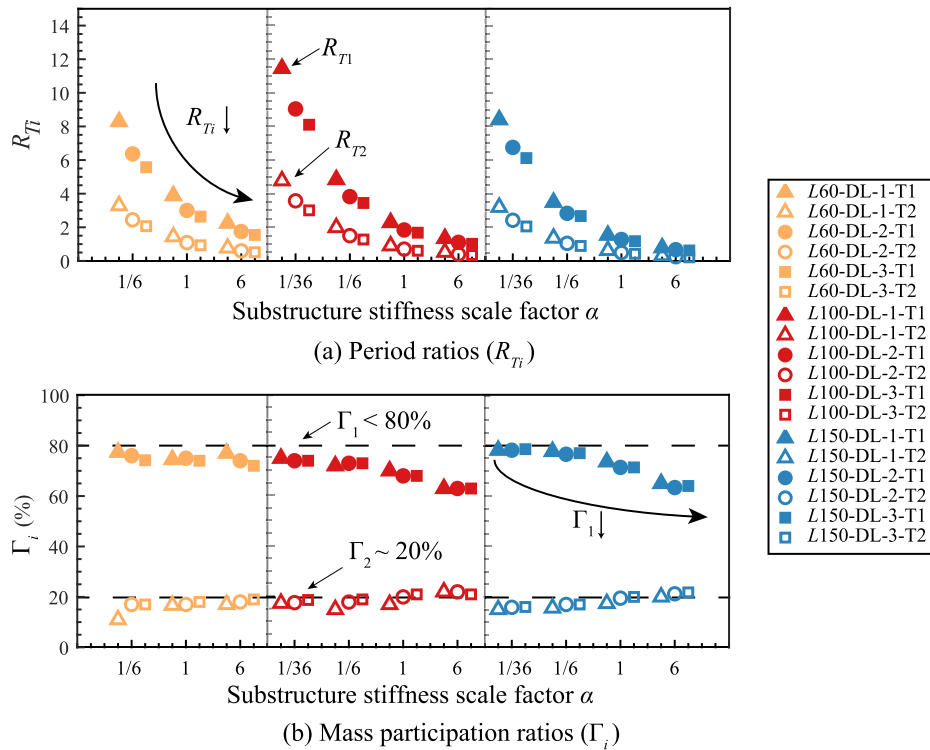


Fig. 6. Multistorey models: Effects of varying the mass and substructure stiffness.

Table 8
Multistorey models: Roof and substructure periods (L60 models).

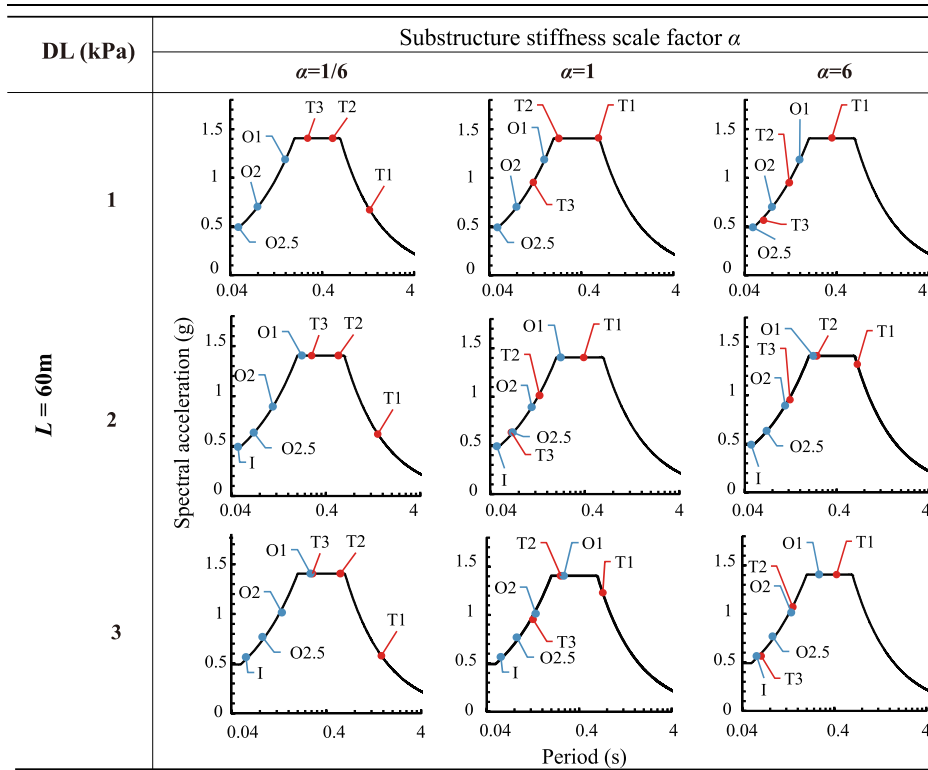
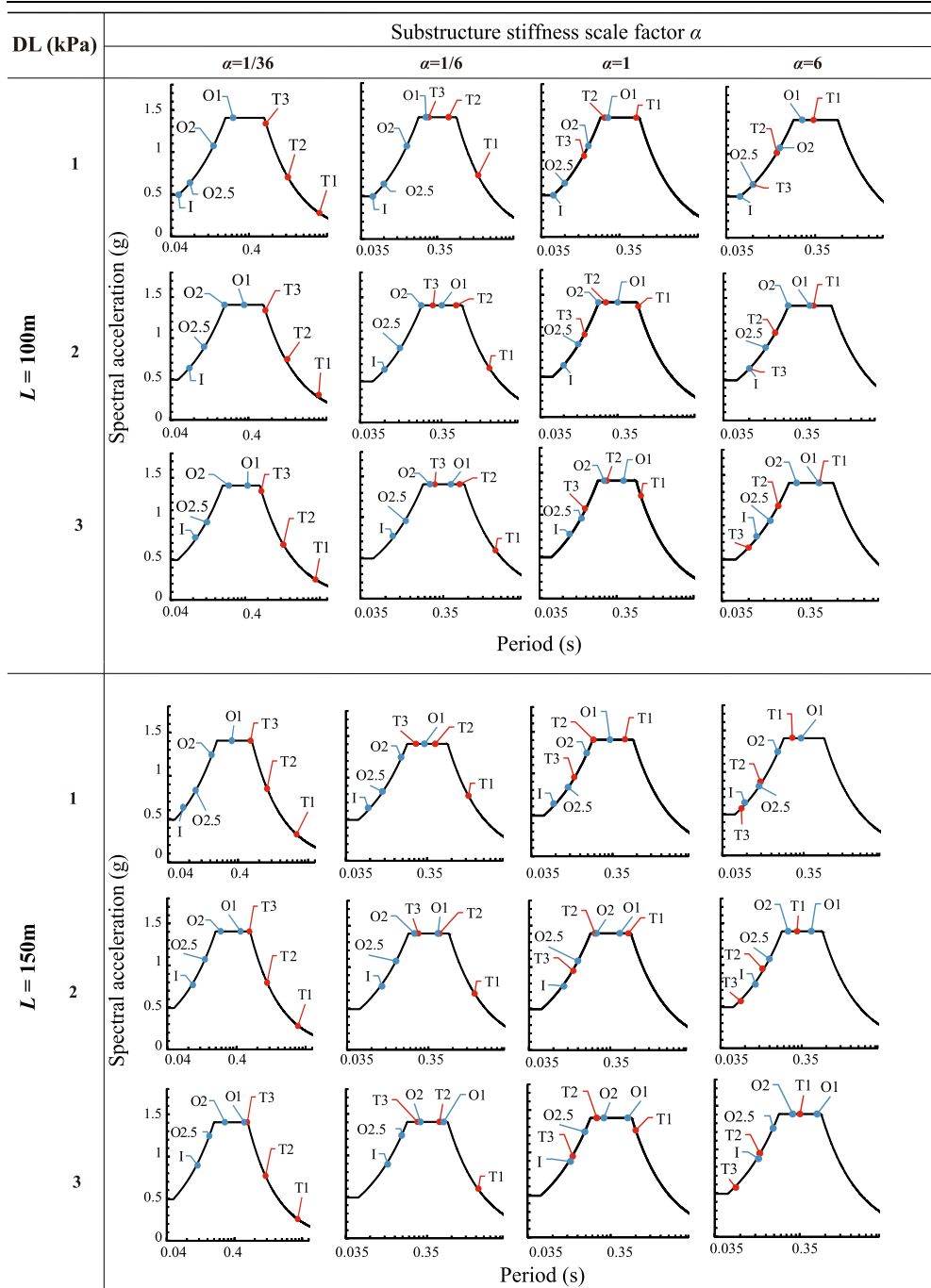


Table 9
Multistorey models: Roof and substructure periods ($L100$ and $L150$ models).



most flexible multistorey substructures ($R_{T1} \gg 2$). For flexible substructures, the vertical T2 dominance ratio occasionally dropped due to resonance of higher substructure modes (e.g. T3) with the roof O1 mode. To summarise, the peak horizontal response is always a combination of the T1-roof and T2-roof interactions, while the peak vertical response is primarily governed by the T1-roof interaction for extremely stiff structures, followed by a combination of the T1-roof and T2-roof interactions for moderately stiff substructures and negligible interaction for flexible substructures.

5. Amplification factors for higher substructure mode

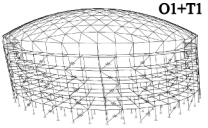
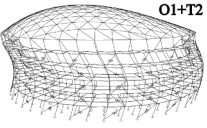
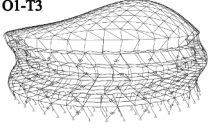
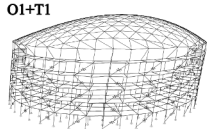
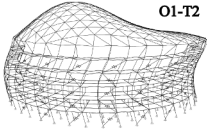
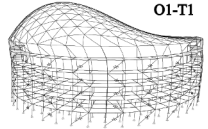
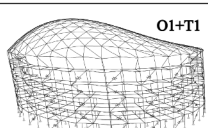
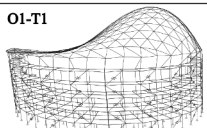
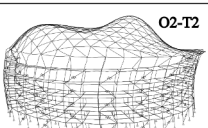
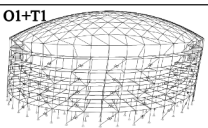
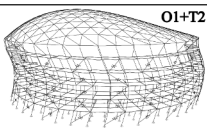
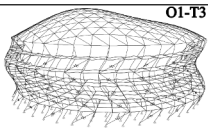
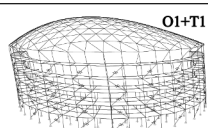
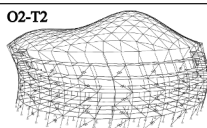
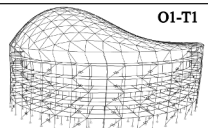
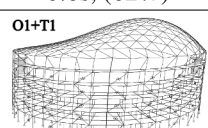
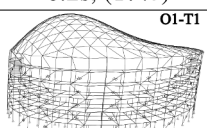
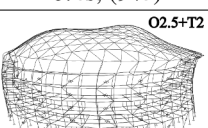
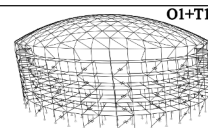
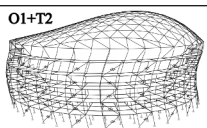
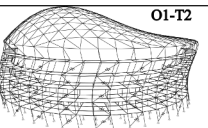
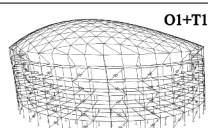
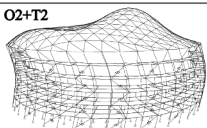
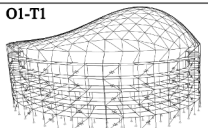
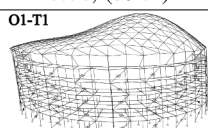
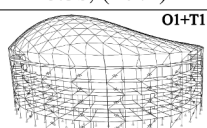
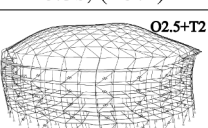
Before quantifying the T2-roof interactions, the following section

reviews the previously proposed amplification factors for T1-roof interactions.

5.1. Substructure T1 mode amplification factor

The T1-roof interactions are characterised by the amplification factors F_{H1} and F_{V1} [24] given by Eq. (11). Note that a vertical calibration factor $C_v\theta$ (Eq. (11)) of 1.85θ was previously proposed based on a numerical study investigating the influence of the half-subtended angle on the peak vertical acceleration [24].

Table 10
Multistorey combined models: Periods (s), mass participation (%) and mode shapes.

DL	R_M	α	$L=100\text{m}$, Mode shapes		
1	11.5	1/6	 1.2s, (73%)	 0.5s, (18%)	 0.2s, (5%)
		1	 0.5s, (68%)	 0.2s, (15%)	 0.3s, (8%)
		6	 0.3s, (49%)	 0.2s, (14%)	 0.1s, (12%)
2	6.2	1/6	 1.3s, (72%)	 0.5s, (18%)	 0.3s, (6%)
		1	 0.6s, (62%)	 0.2s, (17%)	 0.4s, (9%)
		6	 0.4s, (30%)	 0.3s, (29%)	 0.1s, (19%)
3	4.5	1/6	 1.5s, (71%)	 0.6s, (16%)	 0.5s, (6%)
		1	 0.7s, (59%)	 0.3s, (17%)	 0.5s, (10%)
		6	 0.4s, (32%)	 0.5s, (25%)	 0.2s, (21%)

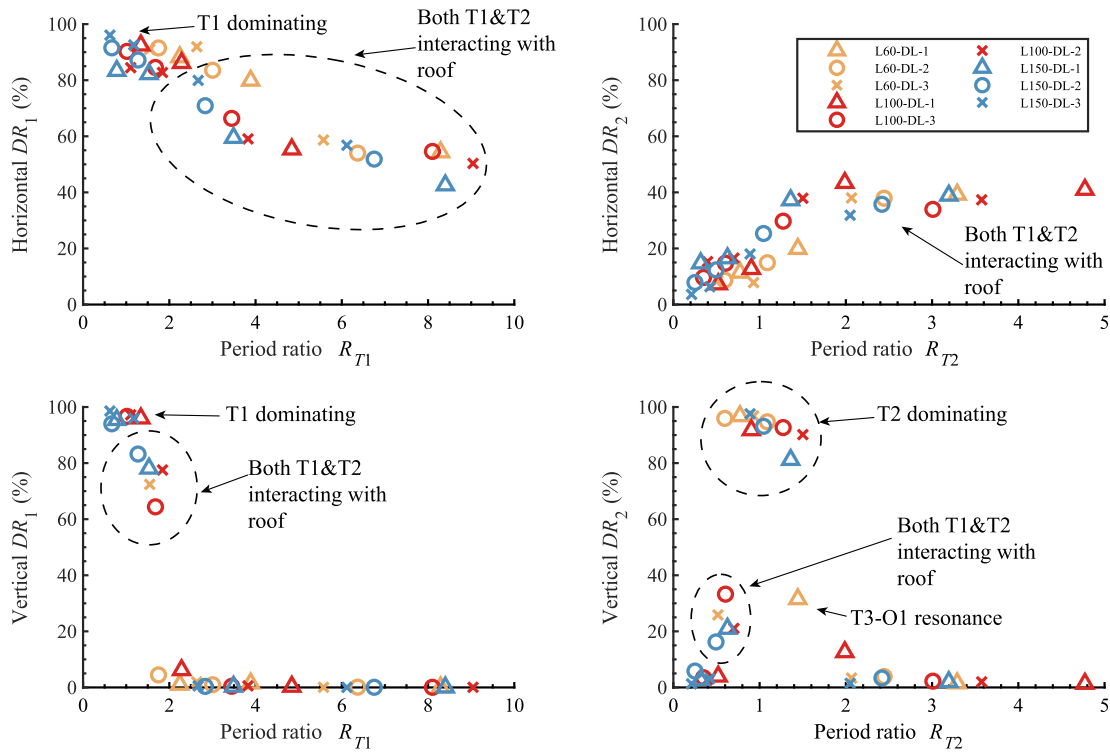


Fig. 7. Dominance response ratios as a function of period ratios.

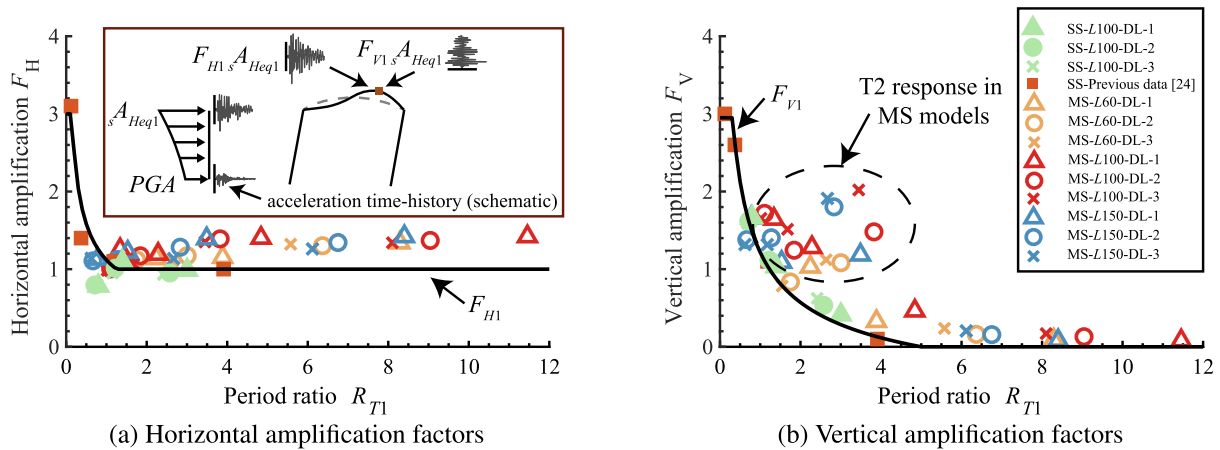


Fig. 8. L100 single-storey(SS) and multistorey(MS) models' response compared to the previous proposal.

$$F_{H1} = \begin{cases} 3 & (0 < R_{T1} \leq 5/36) \\ \sqrt{5/(4R_{T1})} & (5/36 < R_{T1} \leq 5/4) \\ 1 & (5/4 < R_{T1}) \end{cases} \quad (11a)$$

$$F_{V1} = \begin{cases} 3C_v\theta & (0 < R_{T1} \leq 5/16) \\ (\sqrt{5/R_{T1}} - 1)C_v\theta & (5/16 < R_{T1} \leq 5) \\ 0 & (5 < R_{T1}) \end{cases} \quad (11b)$$

$$F_H = \frac{cA_{Hmax}}{sA_{Heq1}}, \quad F_V = \frac{cA_{Vmax}}{sA_{Heq1}} \quad (12)$$

where,

$$sA_{Heqi} = s\beta_{is}S_{dis}\phi_i \quad (13)$$

Fig. 8 compares the previously proposed amplification factors to the results obtained using Eqs. 12 and 13, plotting both against the T1 period ratios. Although the single-storey (SS) models are in good

agreement with the previous proposal (Fig. 8), the multistorey (MS) models exhibit significantly higher amplification factors, especially in the vertical direction for $R_{T1} > 2$. This excess response may be attributed to the amplification arising from the substructure T2 mode, which is close to the roof's predominant modes in this region (Fig. 7). This reiterates the need to characterise the T2-roof interactions and incorporate them in the amplification factor for multistorey substructures.

5.2. Substructure T2 mode amplification factor

To quantify the relationship between amplification factors F_{H2} and F_{V2} and the period ratio R_{T2} (obtained following Eq. 6), the higher mode amplification factors were back-calculated by subtracting the fundamental substructure T1 mode response ($F_{H1s}A_{Heq1}$ and $F_{V1s}A_{Heq1}$) from the combined peak responses (cA_{Hmax} and cA_{Vmax}) obtained from RSA. The CQC rule was adopted and a sufficient number of modes were

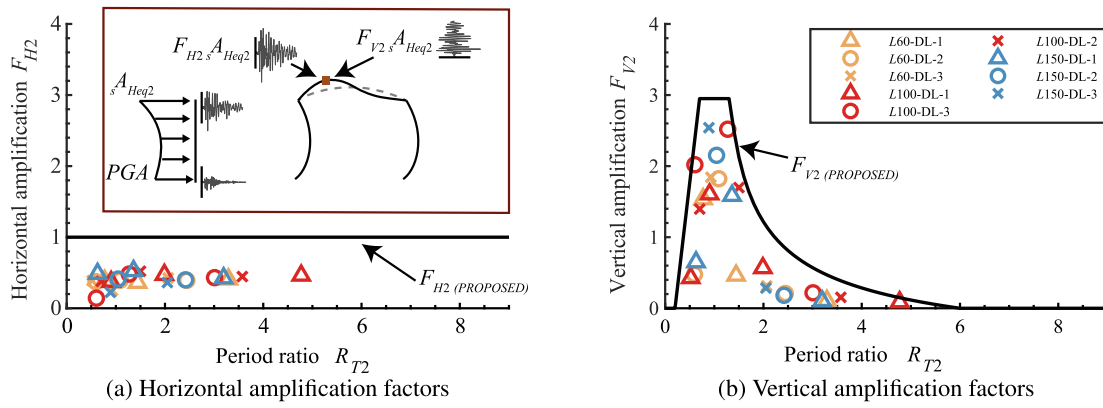


Fig. 9. Proposed amplification factors for higher mode.

considered to achieve at least a 90% combined translational modal mass participation. To accurately capture the response only from the T2 mode, participation from higher substructure T3 or T4 modes were not considered. This excess response was then divided by the peak response of the substructure T2 mode (sA_{Heq2}), as given by Eq. (14). The peak substructure responses sA_{Heq1} and sA_{Heq2} were calculated using the spectral accelerations S_{ai} and Eq. 13. The resulting amplification factors are plotted in Fig. 9 and compared to the proposed substructure T2 mode amplification factors, which are given in Eq. (15) as a function of the period ratio R_{T2} .

$$F_{H2} = \frac{cA_{Hmax} - F_{H1}sA_{Heq1}}{sA_{Heq2}} \quad (14a)$$

$$F_{V2} = \frac{cA_{Vmax} - F_{V1}sA_{Heq1}}{sA_{Heq2}} \quad (14b)$$

$$F_{H2} = 1 \quad (15a)$$

$$F_{V2} = \begin{cases} 0 & R_{T2} \leq 1/5 \\ \frac{6C_V\theta(R_{T2} - 1/5)}{3C_V\theta} & 1/5 < R_{T2} < 7/10 \\ \left(\frac{\sqrt{5/(R_{T2} - 1)} - 1}{\sqrt{5/(R_{T2} - 1)} - 1} \right) C_V\theta & 7/10 \leq R_{T2} \leq 21/16 \\ C_V\theta & R_{T2} > 21/16 \end{cases} \quad (15b)$$

The horizontal response amplifications F_{H1} were sufficiently conservative to cover the mild amplification arising from the substructure T2 mode and so a constant amplification factor of $F_{H2} = 1$ is proposed (Fig. 9). However, significant amplification is observed in the vertical direction, which may be interpreted as the F_{V1} - R_{T1} (Fig. 8) distribution shifted to the right. The plateau region of this curve (Fig. 9) is primarily attributed to the substructure T2 mode interacting with the roof O1 or O2 modes. For extremely stiff substructures with $R_{T2} < 0.2$, F_{V1} tends to cover the mild T2-roof interactions, and so it is proposed to set the vertical amplification of the substructure T2 mode to zero in this region and gradually increase to a peak at $R_{T2} \approx 1$. This may also be seen in Fig. 7, where the vertical DR_2 reduces to zero and the vertical DR_1 almost reaches unity for $R_{T1} < 1$, indicating a dominant substructure T1 response. For a longer R_{T2} , F_{V2} gradually decreases to zero as the T2 mode and roof modes spread further apart, decreasing the interaction and amplification.

5.3. Resonance effect with high mass ratios

Large-scale gymnasiums and auditoriums are typically designed with steel roofs and reinforced concrete substructures, which tend to be heavier than steel frames, resulting in larger substructure mass ratios R_M . Heavy substructures with $R_{T1} < 1.5$ produce significant resonant amplification between the T1 and O1 modes, increasing both the horizontal and vertical responses, as noted by Takeuchi et al. [24]. This has

been accounted for by modifying the amplification factors to F'_{H1} and F'_{V1} when $R_{M1} > 2$, as given by Eq. (16) [24].

$$F'_{H1} = \sqrt{F_{H1}^2 + \frac{1}{(1 - R_{T1}^2)^2 + (1/R_{M1})^\theta}} \quad (16a)$$

$$F'_{V1} = \sqrt{F_{V1}^2 + \frac{1}{(1 - R_{T1}^2)^2 + (1/R_{M1})}} \quad (16b)$$

Domes with multistorey substructures have even heavier substructures, which result in larger mass (typically $R_{M1} > 4$) and period ratios (typically $R_{T1} > 2$) than single-storey substructures. This means that the substructure T1 and roof O1 modes are farther apart, reducing the potential for resonance with the substructure T1 mode. However, R_{T2} may be close to 1, suggesting that the substructure T2 mode may be in resonance with the roof O1 mode. To investigate the T2-O1 resonance effects in structures with heavy substructures, three additional $L = 100$ or 150 m models were constructed with the substructure floor loads increased to 20 (L100-DL-1- R_{M2} -6), 30 (L150-DL-1- R_{M2} -7) or 60 kPa (L150-DL-1- R_{M2} -13), which resulted in mass ratios of about $R_{M1} = 23, 25$ and 49 for the substructure T1 modes, and $R_{M2} = 6, 7$ and 13 for the substructure T2 modes, respectively.

The back-calculated substructure T2 mode amplification factors from Eq. (14) are compared to Eq. (15) in Fig. 10. For $R_{T2} \approx 1$, the proposed curves (Eq. (15)) are conservative enough to cover the mild T2-O1 resonance effects arising in the high R_{M2} models. Therefore, additional amplification for T2-O1 resonance is not required for domes with multistorey substructures and high mass ratios.

5.4. Proposed design procedure to estimate peak response

This section summarises the proposed design procedure (Fig. 11) to obtain the peak roof accelerations and equivalent static forces for the preliminary seismic design of roofs with multistorey substructures.

1. Perform eigenvalue analysis of the substructure and roof models (Fig. 2(a) and 2(b)) to obtain the substructure T1 and T2 modes and roof O1 mode. The cumulative mass participation (Γ_1 in Eq. (7)) from the first two substructure modes should be at least 90%. If the mass participation from the first substructure mode exceeds 90%, the effect of T2-roof interactions need not be considered (i.e. sA_{Heq2} may be taken as 0).
2. Calculate the peak accelerations (sA_{Heqi}) for the two substructure modes using Eq. 13.
3. Calculate the period (R_{T1}, R_{T2}) and mass (R_{M1}, R_{M2}) ratios from Eq. 6. Apply these ratios to compute the roof amplification factors F_{H1} (or F'_{H1}), F_{H2} , F_{V1} (or F'_{V1}) and F_{V2} using Equations (11), (15), and (16).

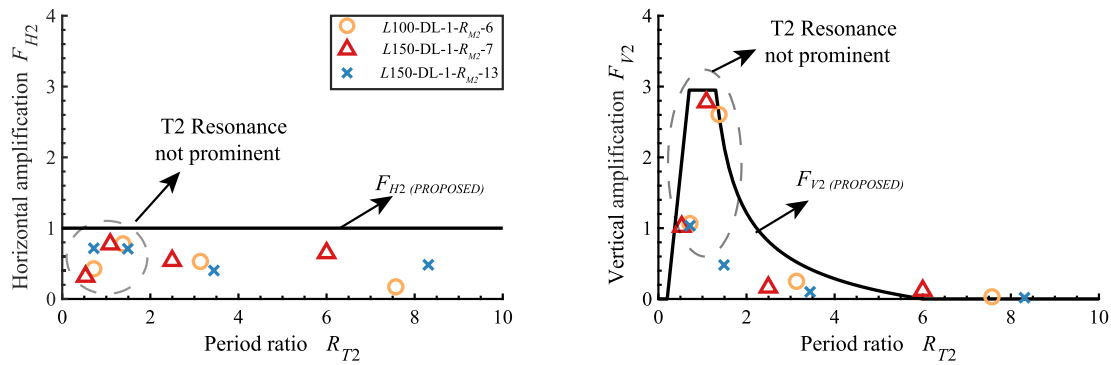


Fig. 10. Effect of high mass ratio R_{M2} on higher mode amplification.

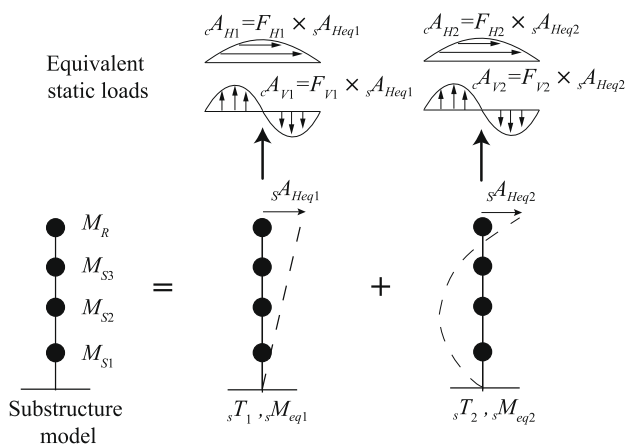


Fig. 11. Simplified method to estimate static loads for domes.

4. Compute the amplified horizontal (cA_{Hi}) and vertical (cA_{Vi}) accelerations to the roof according to the mode-specific distributions. The dominant roof O1 mode is adopted for the envelope, which has the distributions given by (Eqs. (17) and (18)) [24], where x and y are the coordinates of roof nodes, the roof center is located at $\{x, y\} = \{0, 0\}$ and L is the span of the dome.

$$cA_{Hi}(x, y) = sA_{Heq1} \left\{ 1 + (F_{Hi} - 1) \cos \frac{\pi \sqrt{x^2 + y^2}}{L} \right\} \quad (17)$$

$$cA_{Vi}(x, y) = sA_{Heq1} F_{Vi} \frac{x}{\sqrt{x^2 + y^2}} \sin \frac{2\pi \sqrt{x^2 + y^2}}{L} \quad (18)$$

5. Combine the modal accelerations at each node using Eq. (19) to obtain the combined response envelope. This study uses an absolute summation rule. The equivalent static seismic forces for each node may then be computed from the nodal mass m_k and acceleration $cA_H(x, y)$ or $cA_V(x, y)$ at position (x, y) using Eq. (20).

$$cA_H(x, y) = \sum_{i=1}^2 |cA_{Hi}(x, y)| \quad (19a)$$

$$cA_V(x, y) = \sum_{i=1}^2 |cA_{Vi}(x, y)| \quad (19b)$$

$$f_H(x, y) = m_k cA_H(x, y) \quad (20a)$$

$$f_V(x, y) = m_k cA_V(x, y) \quad (20b)$$

5.5. Results

The proposed method was applied to obtain the overall peak response for each model. The detailed results for the L150-DL-1 model are shown in Fig. 12. The individual modal contributions from the response spectrum analyses (labelled ‘RSA T1’ and ‘RSA T2’) are also compared with the proposed equivalent static responses (labelled ‘Proposed T1’ and ‘Proposed T2’).

Models with flexible substructures ($\alpha = 1/36$) produced relatively small roof responses due to the long substructure periods. The flat horizontal response envelope indicates minimal amplification, while the vertical response is almost negligible. Thus, the horizontal acceleration input from the substructure is more significant in these cases. Note that the models with $R_{T2} > 2$ have fundamental periods of around 3s (Fig. 6 and Table 9), which is unusual for shorter multistorey substructures but may occur for taller buildings supporting roofs at height. Models with slightly less flexible substructures ($\alpha = 1/6$) exhibited a vertical roof response dominated by the T2 mode interaction. These are representative of yielded substructures with an elongated first mode. Models with stiffer substructures ($\alpha = 1$) generated a response combining the substructure T1 and T2 modes. In these two cases, the exclusion of the T2 mode will underestimate the response. As the substructure stiffness is further increased ($\alpha = 6$), the vertical response becomes much larger and the response is dominated by T1 mode, while retaining a modest contribution from the substructure T2 mode. The proposed method is thus in good agreement with the actual response over this full range of substructure stiffness.

The proposed equivalent static loads (Eq. (20)) were applied to the roof model (Fig. 2(a)) and the equivalent static analysis results compared to the RSA response of the combined model (Fig. 2(c)). For comparison, results accounting only for the substructure T1 mode (sA_{Heq1}) with the corresponding roof amplification factors (F_{H1} and F_{V1}) are also shown and labelled ‘T1’. This is representative of the method presented in the current IASS design guideline [21], which estimates the equivalent static loads from the roof’s interactions with the first substructure mode alone. The results including the higher mode contributions are labelled ‘T1 + T2’. The improvement in estimation may be measured by comparing the parameters r_{fT1} and r_{fT1+T2} in Eq. (21) which are defined as the median ratios of the responses obtained from the static analyses by the proposed method (r_{T1} and r_{T1+T2}) to the responses obtained from the response spectrum analyses (r_{RSA}) calculated for all the roof members. $r_f < 1$ suggests that the response obtained from the equivalent static loads underestimate the actual response and similarly, $r_f > 1$ indicates a conservative estimate of the response. The estimates for the L100 models are listed and the values for the $\alpha = 1$ models are compared in bar-plots for all the four response parameters in Fig. 13. It was observed that only considering T1 mode severely underestimates the responses for all cases with r_{fT1} around 0.5 except for $\alpha = 6$ models where the substructure first mode dominates the response and $r_{fT1} > 1$. The bending moments were generally the most

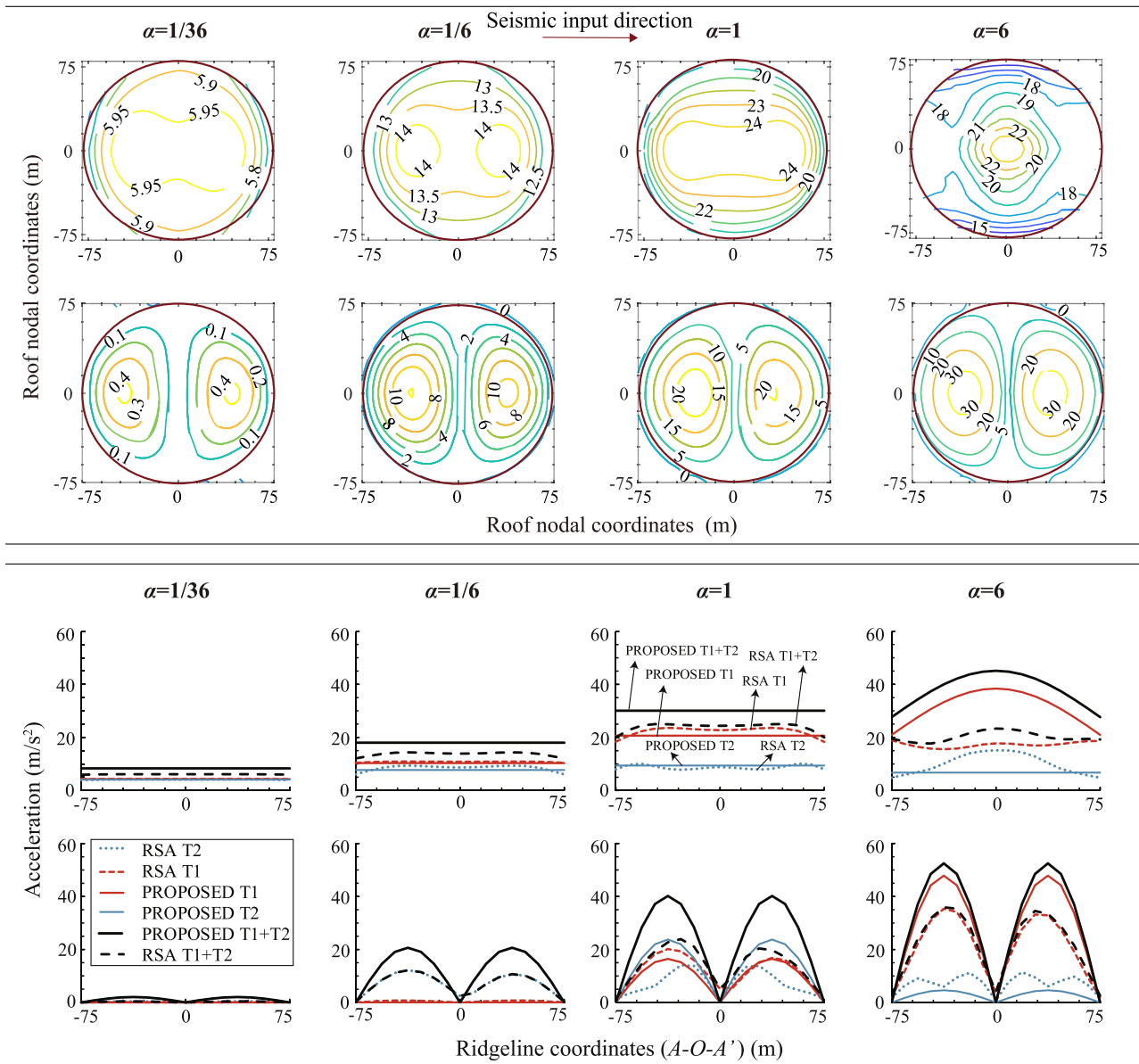


Fig. 12. (a) RSA response: Contour plot of horizontal (top) and vertical (bottom) accelerations (m/s^2). (b) Comparison with proposed response: Horizontal (top) and vertical (bottom) accelerations.

underestimated, and the axial forces the least. Adding the T2 mode's contribution improved this value by as much as 200% for the flexible $\alpha = 1/6$ models and the smallest improvements of around 30% were observed for the stiff $\alpha = 6$ models with the responses for all the cases generally conservative ($r_{T1+T2} > 1$).

$$r_{T1} = \text{median} \left(\frac{r_{T1}}{r_{RSA}} \right) \tag{21a}$$

$$r_{T1+T2} = \text{median} \left(\frac{r_{T1+T2}}{r_{RSA}} \right) \tag{21b}$$

where r is the response parameter: Dh = Horizontal displacement, Dv = Vertical displacement, N = Axial force and M = Bending moment.

The member responses of L100-DL-2 model are also compared in detail in Fig. 14. For $\alpha = 1/6$, considering the contribution from T2 mode increased the accuracy of both the horizontal and vertical displacement responses by about 50%. Similarly, for $\alpha = 1$ model, there was an improvement of 40% in the accuracy of the horizontal and vertical displacement responses when compared to the estimated response

only considering T1 mode. Further, adding the contribution of T2 mode reduced the number of members with underestimation in the forces. Considering just the T1 mode underestimated the axial forces of 68% of the roof members and bending moments of 99% of the members. The current proposal of combining T1 and T2 showed significant improvements in these values with just 8% and 28% of the members with underestimated axial forces and bending moments respectively. This suggests that the bending moments have greater variation and are more sensitive to the excited mode shapes of the roof. For very stiff substructures where $\alpha = 6$, the T1 mode dominates the response and the current guideline of using T1 mode results in sufficiently conservative response estimates with just about 11% of the bending moments being underestimated and 2% of the axial forces. Considering the relatively small contribution of T2 mode resulted in slightly more conservative estimates of the member responses. Thus, including the higher substructure T2 mode (sA_{Heq2}) using the corresponding roof amplification factors (F_{H2} and F_{V2}) significantly increases the accuracy of the member responses by providing a more conservative response, especially for models with $1/6 < \alpha < 1$ (Fig. 14), which is the expected range for

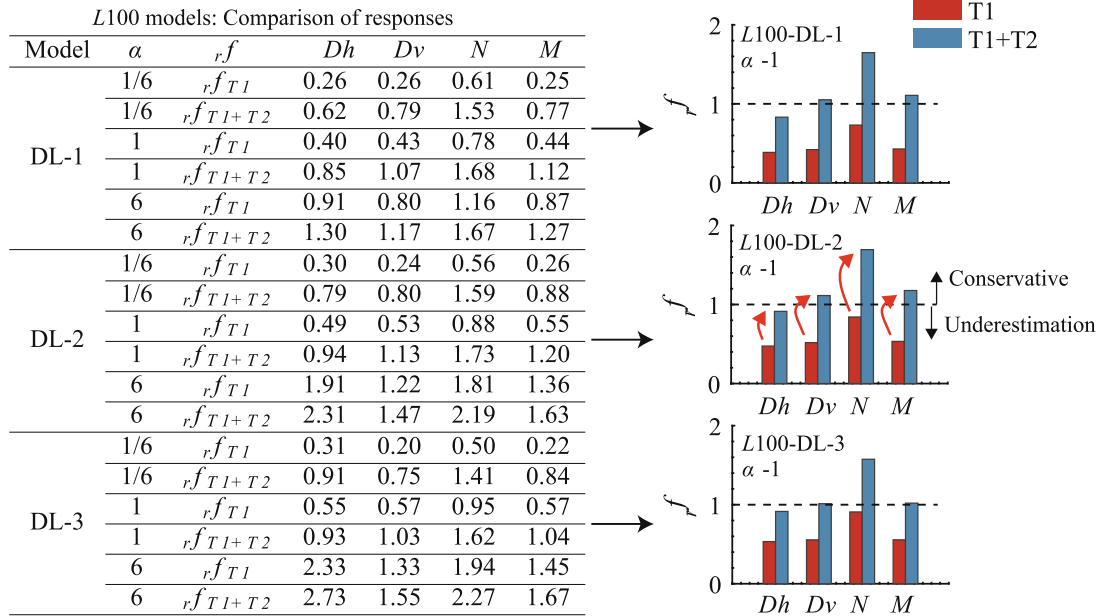


Fig. 13. L100 models: Comparison of response estimation methods.

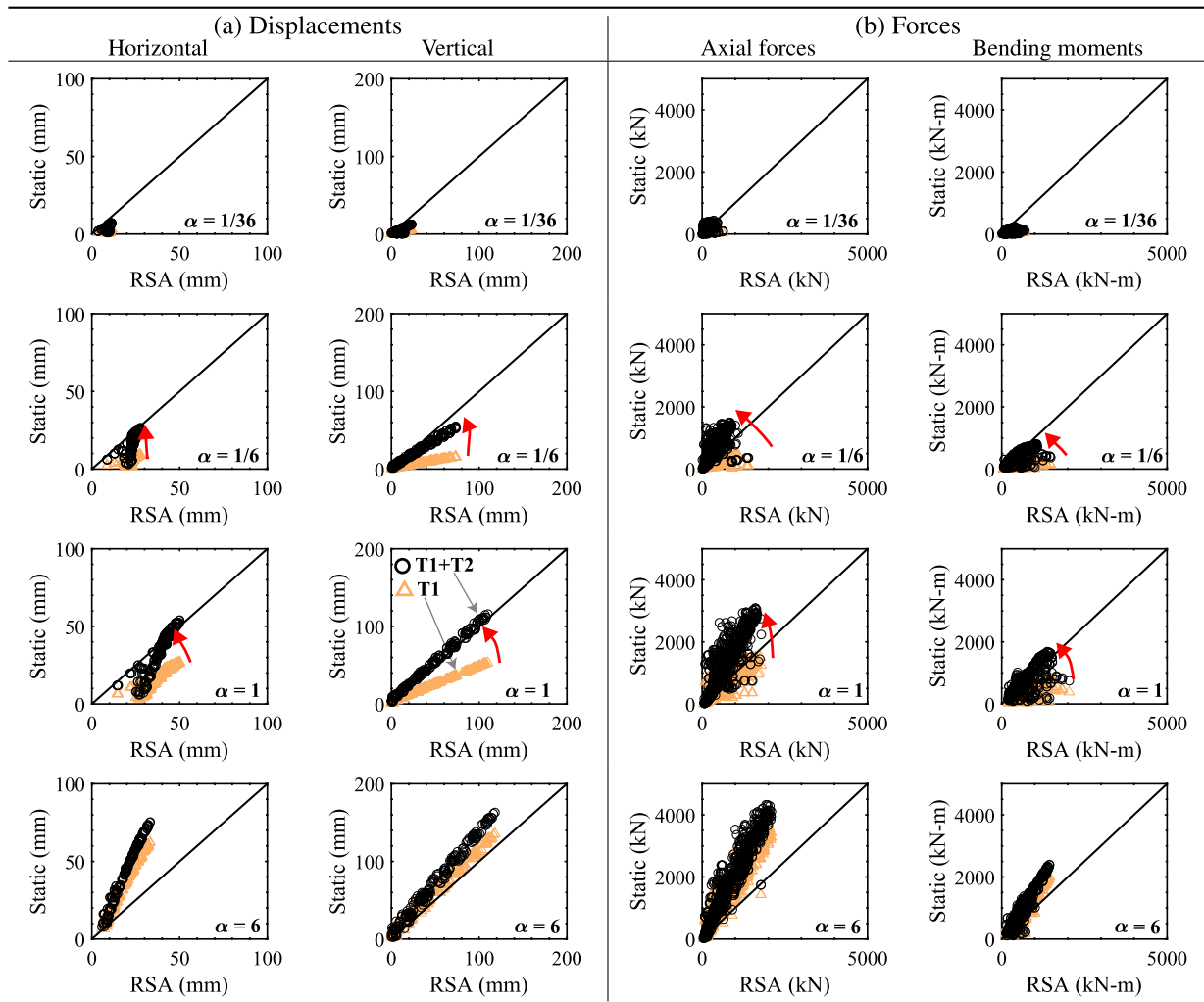


Fig. 14. L100-DL-2 model: Comparison of proposed response with and without higher mode effects.

realistic multistorey substructures. Note that the complexities of a yielding multistorey substructure were omitted, which may be an area of further study.

6. Conclusions

This paper investigated the effects of higher modes of multistorey substructures on the seismic response of dome gridshell roofs using response spectrum analysis. Horizontal and vertical amplification factors were proposed to quantify the interaction between the roof and higher multistorey substructure modes.

The following conclusions were drawn from this investigation:

1. The dominant modes depend on the proximity of the dominant substructure and roof mode periods, with the substructure T1 and T2 modes typically combining with the nearest roof mode. Flexible multistorey substructures ($\alpha = 1/6$ and $\alpha = 1/36$) are governed by the roof O1 mode interacting with the closest substructure mode, while the higher roof modes remain unexcited. Stiffer multistorey substructures ($\alpha = 1$ and $\alpha = 6$) with the T1 and T2 modes close to the roof O1 mode exhibit complex roof-substructure interaction, with significant excitation of the O1, O2, O2.5 and I roof modes.
2. The relative contributions of the substructure T1 and T2 modes to the combined acceleration response were investigated using a dominance response ratio, which includes both the spectral acceleration and mass participation effects. The influence of T2 mode on the vertical acceleration response was found to peak when period ratio $R_{T2} \approx 1$ as T2 dominance ratio DR_2 peaked at almost 100% and became negligible for longer substructure periods with $R_{T2} \gg 2$. The contribution to horizontal response was investigated using the horizontal dominance ratios which were more evenly divided between the T1 and T2 modes for longer period substructures, while the T1-roof interaction dominated for stiff substructures with $R_{T1} < 2$, achieving a horizontal T1 dominance ratio of $DR_1 > 80\%$.
3. The vertical response amplification was found to be sensitive to the period ratios of the T1 and T2 modes to the roof O1 mode (R_{T1} and R_{T2}) with peak amplification from the T2 mode F_{V2} reaching up to a value of 3 as R_{T2} approached 1. The horizontal response amplification (F_H) was primarily a result of the substructure T1 interacting with the roof's predominant modes (F_{H1}) while the peak amplification contribution from T2 mode towards the horizontal response (F_{H2}) was found to around 1.
4. Single-storey substructures and first-mode dominated substructures may obtain the peak roof response solely from the first substructure mode (the current IASS method), but neglecting higher substructure modes underestimated the peak horizontal and vertical accelerations for all the multistorey substructures with a significant T2 mode ($\alpha < 6$ or $R_{T2} > 0.2$).
5. Simple equations were proposed to account for the amplification induced by the substructure T2 mode based on the T2-roof period ratios and to obtain equivalent static loads for preliminary seismic design, significantly improving upon the current IASS method for multistorey substructures. The greatest benefit was for substructures with dominant T2 modes ($1/6 < \alpha < 1$ and $0.2 < R_{T2} < 2$), reducing the percentage of roof members with underestimated forces from around 70% to 6%, while it produced similar accuracy for stiffer first mode dominated substructures ($\alpha = 6$), where the T1 mode's contribution alone produced a conservative response estimate.

Declaration of Competing Interest

The authors declare that they have no known competing financial

interests or personal relationships that could have appeared to influence the work reported in this paper.

References

- [1] Forman SE, Hutchinson JW. Buckling of reticulated shell structures. *Int. J. Solids Struct.* 1970;6(7):909–32.
- [2] Bulenda T, Knippers J. Stability of grid shells. *Computers & Structures* 2001;79(12):1161–74.
- [3] Yamada S. Buckling load evaluation method for single layer cylindrical lattice shells. *Journal of Civil Engineering and Architecture* 2012;6(3):268.
- [4] W.G. 8, Guide to buckling load evaluation of metal reticulated roof structures, Rep Act IASS WG 8 (2014) 10.
- [5] Shen S, Xing J, Fan F. Dynamic behavior of single-layer latticed cylindrical shells subjected to seismic loading. *Earthquake Engineering and Engineering Vibration* 2003;2(2):269–79.
- [6] Cedrón F, Elghazouli A. Seismic performance of single layer steel cylindrical lattice shells. *J. Constr. Steel Res.* 2019;163:105772.
- [7] K. Kawaguchi, Damage to non-structural components in large rooms by the Japan earthquake, in: Structures Congress 2012, 2012, pp. 1035–1044.
- [8] T. Sasaki, A. Aoi, K. Kajiwara, H. Tagawa, D. Sato, Collapse mechanism of wide-area suspended ceiling in school gymnasium, in: Proceedings of IASS Annual Symposia, Vol. 2016, International Association for Shell and Spatial Structures (IASS), 2016, pp. 1–10.
- [9] T. Takeuchi, Y. Terazawa, S. Inanaga, R. Matsui, Collapse analysis of damaged space-frame gymnasiums in the 2016 Kumamoto earthquake, in: Proceedings of IASS Annual Symposia, Vol. 2018, International Association for Shell and Spatial Structures (IASS), 2018, pp. 1–7.
- [10] Zhang Y, Zhi X, Fan F. Fragility analysis of reticulated domes subjected to multiple earthquakes. *Eng. Struct.* 2020;211:110450.
- [11] Zhi X-D, Fan F, Shen S-Z. Failure mechanisms of single-layer reticulated domes subjected to earthquakes. *Journal of the International Association for Shell and Spatial Structures* 2007;48(1):29–44.
- [12] Nie G-B, Zhi X-D, Fan F, Dai J-W. Seismic performance evaluation of single-layer reticulated dome and its fragility analysis. *J. Constr. Steel Res.* 2014;100:176–82.
- [13] Pokusiński B, Kamiński M. Lattice domes reliability by the perturbation-based approaches vs. semi-analytical method. *Computers & Structures* 2019;221:179–92.
- [14] Zhong J, Zhi X, Fan F. Sensitivity of seismic response and fragility to parameter uncertainty of single-layer reticulated domes. *International Journal of Steel Structures* 2018;18(5):1607–16.
- [15] Kawaguchi M, Kato S. Metal space structures. *Journal of the International Association for Shell and Spatial Structures* 2001;42:21–6.
- [16] Nakazawa S, Kato S, Takeuchi T, Xue S-D, Lázaro C. State-of-the-art of seismic response evaluation methods for metal roof spatial structures. *Journal-International Association for Shell and Spatial Structures* 2012;53:117–30.
- [17] ASCE Standard-ASCE/SEI 7-16: Minimum Design Loads for Buildings and Other Structures (2016).
- [18] NZS 1170.5: 2004, Structural Design Actions Part 5: Earthquake actions-New Zealand, Wellington, New Zealand: Standards New Zealand.
- [19] British Standard-Eurocode 8: Design of structures for earthquake resistance, Part 1 (2005) 1998–1.
- [20] The Building Standard Law of Japan on CD-ROM, The Building Center of Japan, 2016.
- [21] Guide to earthquake response evaluation of metal roof spatial structures, Working Group 8, International Association for Shell and Spatial Structures (IASS), 2019.
- [22] S. Kato, S. Nakazawa, Seismic design method to reduce the responses of single layer reticular domes by means of yielding of substructure under severe earthquake motions, in: Proceedings of IASS 2001, Nagoya, Japan, 2001, p. TP077.
- [23] Kato S, Nakazawa S, Saito K. Two-mode based estimation of equivalent seismic loads and static estimation of dynamic response of reticular domes supported by ductile substructures. *Journal of the International Association for Shell and Spatial Structures* 2006;47:35–52.
- [24] Takeuchi T, Ogawa T, Kumagai T. Seismic response evaluation of lattice shell roofs using amplification factors. *Journal of the IASS* 2007;48:197–210.
- [25] T. Takeuchi, T. Kumagai, H. Shirabe, T. Ogawa, Seismic response evaluation of lattice roofs supported by multistorey substructures, in: Shell and Spatial Structures: Structural Architecture - Towards the future looking to the past. IASS Symposium, Venice, Italy, 2007, p. 362.
- [26] Khalili R, Poursaha M, Abedi K. Behavior factor and displacement amplification factor for the seismic design of single-layer barrel vaults. *J. Constr. Steel Res.* 2020; 169:105987.
- [27] M. Jamshidi, A.E. Ramaji, Seismic Response of Double Layer Lattice Domes., *Caspian Journal of Applied Sciences Research* 4 (5).
- [28] T. Kumagai, T. Takeuchi, T. Ogawa, A. Nakama, E. Sato, Seismic response evaluation of latticed domes with elasto-plastic substructures using amplification factors, in: Proceedings of IASS 2005, Bucharest, Romania, 2005, pp. 383–390.
- [29] Nair D, Terazawa Y, Sittler B, Takeuchi T. Seismic response of long-span domes supported by multi-storey substructures. *Journal of the IASS* 2020;61:140–57.
- [30] M. King, W. Whitby, G. Hanshaw, Design of the Singapore Sports Hub Roof with High Strength Niobium Steel, in: IABSE Symposium Report, Vol. 101, International Association for Bridge and Structural Engineering, 2013, pp. 1–8.

- [31] D. Rutten, Grasshopper3D (2015).
- [32] C. CSI, Analysis reference manual for SAP2000, ETABS, SAFE and CSIBridge, Computers and Structures Inc, Berkeley, CA, USA.
- [33] E.L. Wilson, Three-dimensional static and dynamic analysis of structures.
- [34] K.-J. Bathe, E.L. Wilson, Numerical methods in finite element analysis.
- [35] Becker T, Furukawa S, Mahin S, Nakashima M. Comparison of US and Japanese codes and practices for seismically isolated buildings. In: Structures Congress 2010; 2010. p. 2330–8.
- [36] Takeuchi T, Wada A. Buckling-restrained braces and applications. Japan Society of Seismic Isolation 2017.